

A BIOPHYSICAL MODEL OF MULTIPLE-ITEM WORKING MEMORY: A COMPUTATIONAL AND NEUROIMAGING STUDY

J. MACOVEANU,^{a*} T. KLINGBERG^a AND J. TEGNÉR^{b,c}

^aKarolinska Institute, Neuropediatrics, Astrid Lindgren Children's Hospital, Q2:07, 171 76 Stockholm, Sweden

^bComputational Biology, Department of Physics, Linköping's Institute of Technology, 581 83 Linköping, Sweden

^cKarolinska Institute, Center for Genomics and Bioinformatics, Berzelius väg 35, 171 77 Stockholm, Sweden

Abstract—Biophysically based computational models have successfully accounted for the persistent neural activity underlying the maintenance of single items of information in working memory. The aim of the present study was to extend previous models in order to retain multiple items, in agreement with the observed human storage capacity. This was done by implementing cellular mechanisms known to occur during the childhood development of working memory, such as an increased synaptic strength and improved contrast and specificity of the neural response. Our computational study shows that these mechanisms are sufficient to create a neural network which can store information about multiple items through sustained neural activity. Furthermore, by using functional magnetic resonance imaging, we found that the information-activity curve predicted by the model corresponds to that in the human posterior parietal cortex during performance of working memory tasks, which is consistent with previous studies of brain activity related to working memory capacity in humans. © 2006 IBRO. Published by Elsevier Ltd. All rights reserved.

Key words: neural network models, parietal lobe, developmental mechanisms.

Working memory (WM) is the ability to maintain and manipulate information during brief periods of time. This ability plays a critical role in the execution of complex behavioral tasks (Baddeley and Hitch, 1974). The putative neural correlate of WM is a stimulus selective persistent neural activity observed in prefrontal and posterior parietal cortical areas (Goldman-Rakic, 1995; Wang, 2001). Sustained neural activity in absence of external stimuli was first demonstrated using electrophysiological methods in monkeys performing visuo-spatial working memory (vsWM) tasks (Fuster, 1973; Funahashi et al., 1989). Biophysical network models of spiking neurons have successfully been used to capture the central features of the observed neural activity during vsWM tasks (Tegnér et al., 2002; Wang et al., 2004). This class of models can account for several experimental observations such as spontaneous firing,

persistent activity with physiological firing rates and realistic shape of neuronal tuning curves as measured in monkeys (Constantinidis and Goldman-Rakic, 2002). In consensus with previous findings (Kilner et al., 2005), the network activation during memory maintenance, as revealed by local field potential measurements, is positively correlated with the expression of EEG frequencies within the gamma band and negatively correlated with alpha band frequencies. However, current models have several limitations e.g. low storage capacity, memory drift and sensitivity to distractors (Wang, 2001; Constantinidis and Wang, 2004). In particular, the models can at most retain information about the spatial location of two stimuli (Tanaka, 2002), which is not consistent with the fact that humans retain information about the location of at least four items in vsWM at the same time (Luck and Vogel, 1997; Cowan, 2001). Being based on recurrent connectivity, these models store the memories through self-sustained stable states of persistent activity, also known as bump attractors. However, due to network dynamics balanced by excitatory and inhibitory feedback, recurrent networks have difficulties maintaining more than two concurrent bump attractors. Additional cues will amplify the fast inhibitory feedback and suppress further excitatory activity.

A few other studies have explored the multiple-item ability of WM models in different contexts. Jensen and Lisman (1996) explained the limited capacity of short-term memory with the fixed number of gamma cycles within a theta cycle. Memories were represented by subsets of cells firing in synchrony. Different items are firing during different gamma cycles. In this way a list of maximum seven items can be activated sequentially within a theta cycle. In the framework of strongly recurrent neural networks, Amit and coworkers (2003) encoded distinct cues by an arbitrary number of separate functional neuronal populations respectively.

The aim of the present study was to investigate how several items can be stored in a neural network based on recurrent connectivity. The model stores information about specific stimuli through selective persistent states of neural activity. Similar models have successfully simulated one-item WM in networks of integrate-and-fire neurons (Amit and Brunel, 1997; Wang, 1999; Compte et al., 2000) and have later been extended by Tegnér et al. (2002) to incorporate biophysical mechanisms. It is known that the ability to hold multiple items in WM increases during childhood development (Luna et al., 2004). We therefore implemented putative cellular changes that occur during WM development in the computational WM model studied by

*Corresponding author. Tel: +46-8-517-761-76; fax: +46-8-517-732-66. E-mail address: julian.macoveanu@ki.se (J. Macoveanu).
Abbreviations: BOLD, blood oxygen level-dependent; E cell, excitatory cell; fMRI, functional magnetic resonance imaging; vsWM, visuo-spatial working memory; WM, working memory.

Tegnér et al. (2002), to test if these could increase the storage capacity of the model.

Synaptic remodeling is considered to be a dominant developmental mechanism during childhood (Huttenlocher, 1979). This process is responsible for both the selective strengthening of the inter-neuronal connections between functional related cells and weakening between functionally unrelated cells (Hubel and Wiesel, 1963; Rainer and Miller, 2000). These structural and connectivity changes can be explained by a few hypothetical mechanisms: increased overall excitatory synaptic strength (A), higher contrast of the neuronal response (B), and increased specificity of the neuronal response (C). We implemented these putative cellular changes during development in a biophysical network model and we made qualitative and quantitative evaluations of the generated network responses corresponding to modes A, B and C. Furthermore, the relationship between the stored information and neural activity predicted by the network was tested against data collected during a functional magnetic resonance imaging (fMRI) experiment. The test was performed in order to assess whether there exist areas in the brain that show similar relation between information load and brain activity and to localize these areas.

EXPERIMENTAL PROCEDURES

The computational model

Neurons. The vsWM model, previously described by Tegnér et al. (2002), integrates electrophysiological data about the stimulus specific persistent activity and neuronal firing rates from oculomotor delayed-response tasks (Funahashi et al., 1989; Goldman-Rakic, 1995). The neuron models followed the Hodgkin-Huxley formalism for the membrane conductance and had a realistic action potential profile and neuronal input–output relationship in accordance with cortical-slice studies (McCormick et al., 1985; Markram et al., 1997). The excitatory postsynaptic currents followed the gating kinetics of the NMDA and AMPA receptors (Hestrin et al., 1990; Jahr and Stevens, 1990; Spruston et al., 1995). The inhibitory currents were mediated by the fast GABA_A receptors (Amari, 1977; Salin and Prince, 1996; Xiang et al., 2002). Synaptic currents were modeled according to $I_{syn} = g_{syn}s(V - E_{syn})$, where g_{syn} represents the synaptic conductance, E_{syn} the synaptic reversal potential and s is the gating variable which decides the fraction of open synaptic ion channels. A complete description of the neuronal model can be found in Tegnér et al. (2002).

Network connectivity. The network represents a local cortical circuit with two populations of cells, 256 Excitatory (E) of pyramidal type and 64 Inhibitory (I) of fast-spiking type (Amit and Brunel, 1997; Wang, 1999; Compte et al., 2000; Tegnér et al., 2002). The neurons were spatially distributed in a ring in accordance with their preferred stimulus location (Fig. 1A) resembling previous oculomotor delayed-response task experiments (Funahashi et al., 1989; Goldman-Rakic, 1995). The synaptic connection strength between neurons decreases with the angle between their preferred stimuli location (Fig. 1B). The connectivity W between neuron i and j follows:

$$W(\theta_i - \theta_j) = J^+ + (J^- - J^+) \exp\left(-\frac{(\theta_i - \theta_j)^2}{2\sigma^2}\right)$$

(Compte et al., 2000)

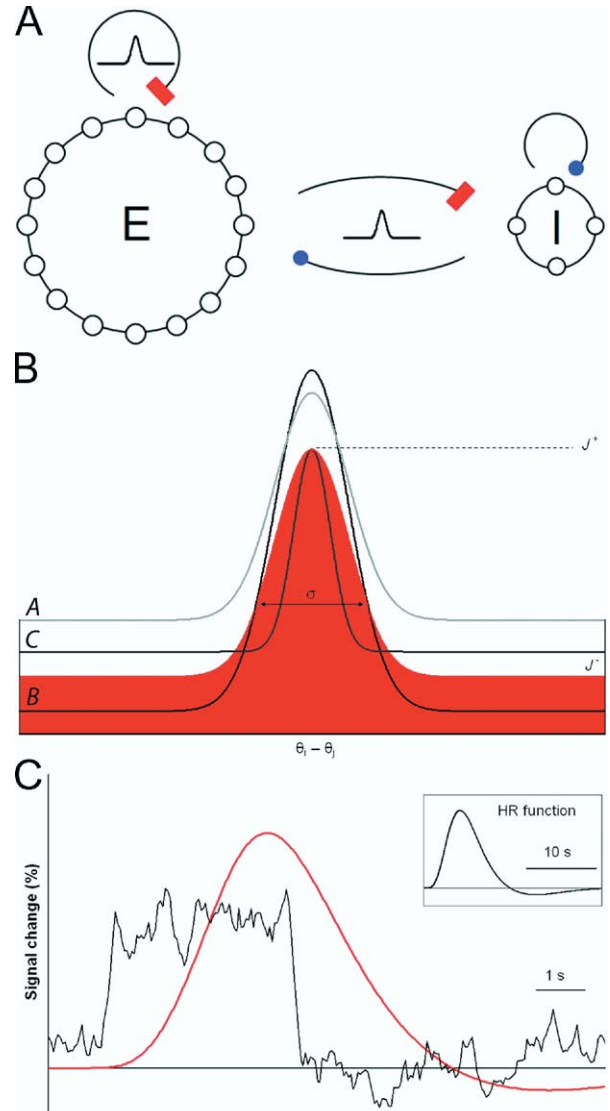


Fig. 1. The recurrent network model. (A) One population of Excitatory (E) and one of Inhibitory (I) cells with all-to-all connections both within and between the populations (illustration not to scale). (B) Connectivity curves between E cells. The initial connectivity for the *Low* mode, shaded area, and after the implemented developmental changes A, B and C. The connectivity strength between E cells depended on their proximity, represented by the angle between them ($\theta_i - \theta_j$). (C) The BOLD signal generated by the network (red curve) is calculated by convolving the total synaptic activity (black trace) with a standard hemodynamic response (HR) function (inset).

$W(\theta_i - \theta_j)$ represents the normalized connectivity. J^- is the strength of the weak distant connections, J^+ the strength of the strong adjacent connections and σ the connectivity footprint. Accordingly, the synaptic conductance is given by: $g_{syn,ij} = W(\theta_i - \theta_j)G_{syn}$.

Network modes. Several modes of the network were evaluated: a reference low capacity mode (*Low*), three modes with one developmental mechanisms implemented, increased overall excitatory synaptic strength (A), higher contrast of the neuronal response (B), and increased specificity of the neuronal response (C), a mode with the highest achievable storage capacity (*High*), and a mode with storage capacity tuned to behavioral data from a

Table 1. Simulation parameters for all network modes

	E→E (NMDA)				All modes		
	G ^a	J ⁺	σ		G ^a	J ⁺	σ
Low	1.55	8	0.16	E→I _(NMDA)	1.16	2	0.5
A	1.71	—	—	I→E _(GABA)	0.47	2	0.7
B	—	15	—	I→I _(GABA)	0.65		
C	—	—	0.07	E _{ext} →E _(AMPA) ^b	0.0104		
High	1.71	15	0.07	E _{ext} →I _(AMPA) ^b	0.0024		
Behavioral	1.63	13	0.09				

^a Conductances are in mS/cm².

^b The external excitation (E_{ext}) from other cortical areas was modeled as uncorrelated Poisson spike trains of 1000 Hz per cell.

vsWM delay-response task (*Behavioral*). The modifications of the network model according to A, B and C were performed by altering the connectivity structure as shown in Fig. 1B. A constant strengthening of the excitatory connections (A) was achieved by increasing the synaptic conductance (G_{EE}) between all excitatory neurons. The contrast of the neural response was increased by increasing the height of the connectivity curve (J⁺) resulting in a selective strengthening of proximate connections and weakening of distant connections (B). Reducing the connectivity footprint (σ), increased the specificity of the neural response leading to faster decrease of the connectivity strength with the inter-neuronal distance (C). The simulation parameters are presented in Table 1.

Simulation of the blood oxygen level-dependent (BOLD) response. The BOLD signal measured with fMRI reflects the total synaptic activity in a brain area (Attwell and Iadecola, 2002). In order to relate simulated neural activity with experimentally measured brain activity, we evaluated a BOLD signal by convolving the total synaptic activity (I_{syn}) of the network model with an experimentally measured canonical hemodynamic response func-

tion modeled by h(t), Fig. 1C. The convolution equation used to evaluate the bold signal b(t) was given by:

$$b(t) = \int_0^t h(t-t') I_{syn}(t') dt'$$

The experimental hemodynamic response was fitted by h(t):

$$h(t) = \frac{\lambda_1^{s_1} t^{s_1-1}}{(s_1-1)!} e^{-\lambda_1 t} - \frac{\lambda_2^{s_2} t^{s_2-1}}{(s_2-1)!} e^{-\lambda_2 t}$$

(Friston et al., 1998)

where t is time and s₁=6, s₂=16, λ₁=λ₂=1/8, r=6 are parameters that calibrate the function for the best fit. I_{syn} was calculated as the sum of the absolute values of the recurrent excitatory currents mediated by NMDA receptors, external excitation through AMPA receptors and the GABA-ergic inhibitory currents (Deco et al., 2004; Deco and Rolls, 2005).

vsWM task protocol: behavior and simulation

Three healthy participants (age 30–32) performed a vsWM task in which they remembered the spatial location of one to six items (Fig. 2). The task was first performed outside (six levels with 10 memory trials for each level) and later in the MR scanner (6×10 memory+6×10 control trials).

The simulation trials followed a similar protocol to the memory trials of the vsWM task. The network model was stimulated by one to six cues given at random locations on the ring, with a minimum of 22.5° between them. The cues consisted of a 0.8 μA/cm² excitatory current injected in 10 adjacent excitatory cells for 1.3 s. The activity traces induced by the cues lasted beyond the stimulation time. The number of bump attractors found at the end of the delay phase represented ‘remembered cues.’

The fMRI experiment

An fMRI experiment was performed in order to measure the BOLD response of the three tested participants while they were perform-

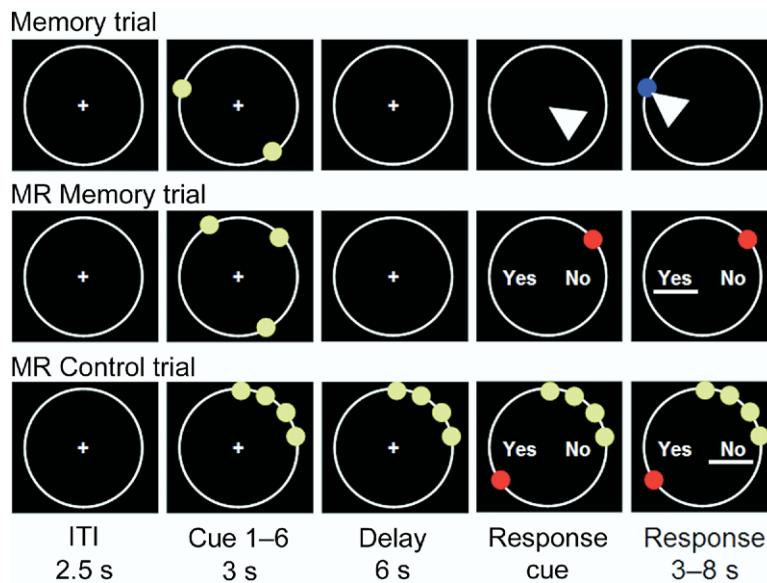


Fig. 2. Schematic representation of the memory and control trials. For the memory trials, between one and six dots were presented simultaneously on a screen, at random locations on the periphery of a circle. The participants tried to remember the location of the dots during a delay phase. At the end of the delay, participants responded using a computer mouse by clicking at all remembered locations. For the trials performed in the MR scanner, the stimuli were back-projected on a screen which the participant viewed through a mirror. A dot appeared during the response phase and they responded by pressing ‘yes’ and ‘no’ buttons if the dot appeared at the same location as a dot presented in the beginning of the trial (½ trials). For the control trials, the stimuli always appeared at the same locations and remained visible during the rest of the trial.

Table 2. (A) Qualitative analyses of the implemented network modes and (B) quantitative differences between the *Low* and *High* modes

	G_{EE}	J_{EE}^+	σ_{EE}	Capacity	BOLD
A					
<i>Low</i>	—	—	—	—	—
<i>A</i>	↑	—	—	↑	↑
<i>B</i>	—	↑	—	↑	↑
<i>A+B</i>	↑	↑	—	↑	↑↑
<i>C</i>	—	—	↓	→	↓
<i>High</i>	↑	↑	↓	↑↑	↑
	Capacity (# items)	BOLD (%)	Distractibility (μ A)	Memory drift	Firing rate (Hz)
B					
<i>Low</i>	2	0.28	1.1	3°	19
↓	↓	↓	↓	↓	↓
<i>High</i>	6	0.57	3.6	2°	26

'Capacity' is the maximum number of items that could be held simultaneously during a 6 s delay. 'BOLD' is the maximum signal change when four items were presented. 'Distractibility' is the least current (induced at 33° distance from the cue) needed to suppress the bump activity. 'Memory drift' is the average drift of a bump attractor after a 6 s delay. 'Firing rate' is the peak firing rate of the bump neurons ($\sigma=0.09$).

ing a vsWM task (Fig. 2). The functional images were acquired by T2*-weighted echo-planar MRI at 1.5 T (TE 40 ms, TR 2000 ms, flip angle 76°, field of view 22 cm, 64×64 matrix). Twenty-two 4.5 mm thick slices were taken with 0.1 mm skip between slices.

The fMRI data were analyzed with SPM2 (www.fil.ion.ucl.ac.uk/spm). The processing included realignment to the first image, correction for movement artifacts, slice-time correction by interpolation to the middle slice, co-registration of the anatomical images to the mean functional image, normalization of the anatomical images to a T2-template and spatial smoothing with an isotropic Gaussian kernel of 8 mm. The general linear model of fMRI time-series (Friston et al., 1995) was applied to analyze the fMRI data with separate conditions for cue presentation, delay, and response selection. Delay-related activity was estimated by contrasting the activity in the six-second delay phase of the WM task and that in the control task.

Model testing

The calculated BOLD values from the simulation experiment were used as covariates in the statistical analyses of the fMRI data in order to find cortical areas that presented a similar pattern of activation as predicted by the computational model.

RESULTS

Our study addresses the limited capability of previous WM network models to explain the experimentally observed WM performance. We have explored the multiple-item capacity of a biophysical WM model by integrating three putative developmental mechanisms. The storage capacity of the network was tuned using behavioral data from a vsWM delay-response task performed by three participants. The same participants performed a similar task in an fMRI experiment and their BOLD signal was measured. The relationship between stored information and neural activity predicted by the WM model was tested against the fMRI data collected, allowing the identification of brain areas that presented similar activation patterns.

Simulated developmental changes

The capacity and BOLD signal of the reference mode (*Low*) were compared with the modes that integrated de-

velopmental changes: *A*, *B*, *A+B*, *C* and *High* (*A+B+C*). Table 2A shows simulation results for the six tested network modes. Independent network simulations according to modes *A* or *B* increased the BOLD response and doubled the storage capacity of the network from two to four items. Implementing simultaneously *A* and *B*, further increased the BOLD response but the storage capacity remained at four items, a constraint imposed by the limited excitation level in the network. A narrower connectivity curve (mode *C*) lowers the excitatory activity reflected by a lower BOLD signal but maintains the storage capacity. In order to achieve the maximum storage capacity of the network, we combined the three tested developmental changes *A*, *B*, and *C* (*High*). Compared with *Low*, the *High* mode had a higher BOLD signal for equal number of presented cues and showed a considerable storage capacity increase (six items). Table 2B summarizes the quantitative differences between the *Low* and *High* modes. The information maintained by the *High* network was both more accurate (lower memory drift) and significantly more resistant to distraction. The higher generated BOLD signal of the *High* mode is related to both a higher number of maintained bump attractors but also to higher firing rate of the bump attractor neurons.

Fig. 3A and B left, shows the spatio-temporal firing pattern of the *Low* and *High* network modes and the calculated BOLD signal (right). Only the *High* mode was capable of maintaining bump activity for all four presented cues until the end of the delay phase.

Network tuning using behavioral data

The average performance, as measured by the number of remembered items (\pm S.E.M.), for the vsWM task performed outside the MR scanner was 1.0 ± 0.0 , 2.0 ± 0.0 , 2.7 ± 0.5 , 3.5 ± 0.8 , 4.0 ± 0.8 , and 3.7 ± 1.0 when the set size increased from one to six presented cues (Fig. 4). The variance between individual performances was low. The average maximum capacity of approximately four remembered cues was attained for a presentation set of five cues.

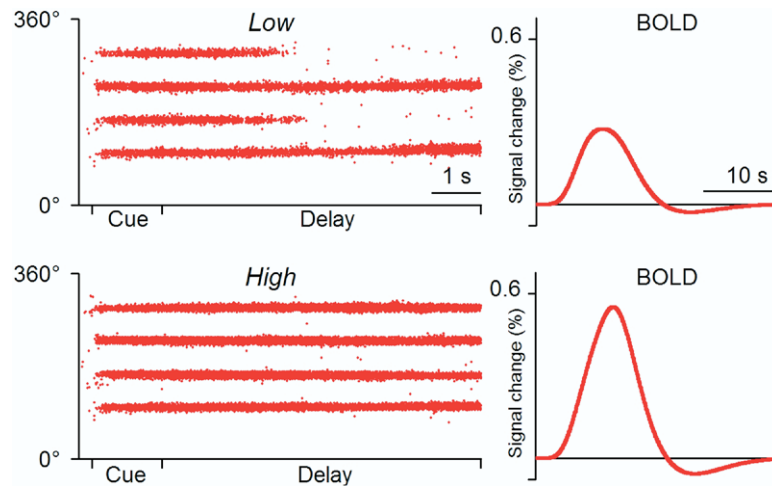


Fig. 3. Network simulations. Left, spatiotemporal firing pattern of *Low* (a) and *High* (b) network modes. The dots correspond to action potentials of pyramidal cells. Both simulations were performed under the same conditions. The four presented cues induce bump attractors through the delay phase. Right, calculated BOLD responses.

The behavioral values were used to tune the storage performance of the network model. Modifying the connectivity structure according to the *A*, *B*, and *C* developmental changes but to a lesser extent than in *High*, we obtained a network mode that exhibited similar performance to the average performance of the tested participants. The BOLD signal of the network mode proved to be highly correlated with the behavioral performance irrespective of the size of the presentation set.

fMRI experiment

Fig. 5 shows areas in which the delay-phase BOLD responses for the three individuals significantly correlated with the simulated BOLD signal, and thus might be inferred as the capacity-related areas ($P < 0.05$, corrected for multiple comparisons). The stereotaxic coordinates of the significantly activated clusters are shown in Table 3. The intraparietal part of posterior parietal cortex showed the highest activation for all tested participants. Additionally,

one participant showed significant right activation and a second participant bilateral activations of the dorsolateral prefrontal cortex. The location of these areas are consistent with previous studies identifying visuo-spatial WM capacity to the intraparietal cortex (Klingberg et al., 2002; Olesen et al., 2003; Todd and Marois, 2004).

DISCUSSION

In general, biophysically realistic vsWM models that integrate experimental data represent a new generation of computational tools essential for understanding the neural mechanism underlying vsWM and its capacity limitations (Jensen and Lisman, 1996; Amit and Brunel, 1997; Compte et al., 2000; Tegnér et al., 2002; Tanaka, 2002; Amit et al., 2003; Deco et al., 2004; Wang et al., 2004). Our study demonstrates the utility of these models by generating experimentally testable predictions.

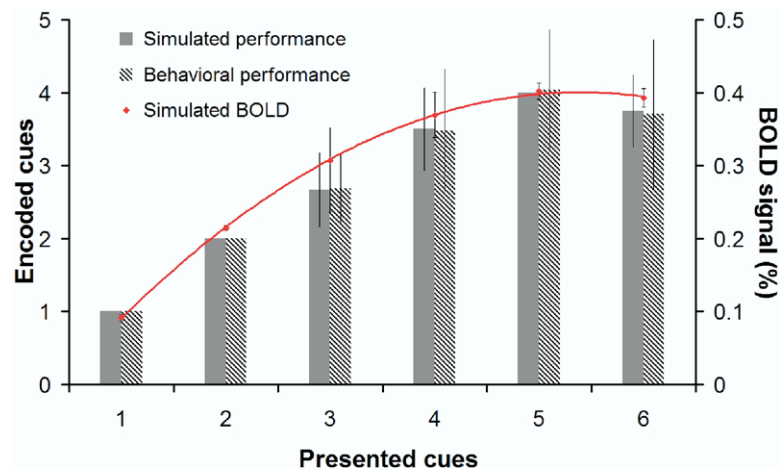


Fig. 4. Behavioral performance and the behaviorally tuned network capacity with corresponding BOLD response function. The bars represent the standard deviation.

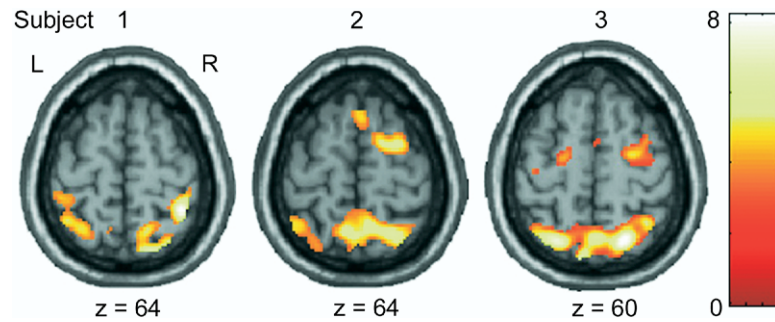


Fig. 5. Correlation maps ($P < 0.05$ corrected) for three individuals superimposed on a standard anatomical template. Images show brain areas with similar relationship between stored information and neural activity as predicted by the vsWM model. The scale bar indicates the significance of the activations (T-values).

In particular, we showed that implementing putative cellular changes during development in a biophysical vsWM model resulted in a substantially increased storage capacity together with a more robust stimuli encoding. The behaviorally measured vsWM performance could be accounted for if all tested changes, increased synaptic strength and improved contrast and specificity of the neuronal response, were implemented simultaneously. The correlation between stored information and neural activity predicted by the network was tested against data collected during an fMRI experiment. We found cortical areas that presented a similar information-activity curve during the delay period of a vsWM task. Both the parietal and frontal areas that were activated by the tested group have previously been associated with vsWM capacity (Klingberg et al., 2002; Olesen et al., 2003; Todd and Marois, 2004). Furthermore, our results (Table 2B) support the correlation between a higher storage capacity, resistance to distractors, mnemonic accuracy, BOLD response and average firing rate of the neuronal populations responsible for the memory maintenance.

Table 3. Individual delay-phase activations

Brain area		MNI coordinates			T score	Size (cm ³)
		x	y	z		
Subject 1						
Intraparietal sulcus	R	38	-44	64	7.3	7.49
Intraparietal sulcus	L	-30	-54	70	5.8	6.99
Superior parietal lobe	R	18	-70	64	6.1	5.05
Subject 2						
Superior parietal lobe ^a	L	-8	-54	72	7.3	29.79
Intraparietal sulcus ^a	R	42	-38	44	6.1	29.79
Middle frontal gyrus	R	42	42	24	6.3	8.07
Superior frontal sulcus	R	26	0	66	5.4	3.60
Subject 3						
Superior parietal lobe ^b	R	22	-64	60	8.2	46.72
Intraparietal sulcus ^b	L	-8	-76	66	7.7	46.72
Middle frontal gyrus	R	58	10	26	5.8	6.60
Middle frontal gyrus	L	-54	-4	38	6.9	5.42

Significant clusters ($P < 0.05$ corrected for multiple comparisons).

^{a,b} The same cluster.

Experimental support for the modeled developmental mechanisms

The implemented changes of the connectivity structure and inter-neuronal connection strengths may serve as a hypothetical model of the developmental changes during childhood. The qualitative differences between the *Low* and *High* network modes can be related to experimental studies of the WM development. Both the WM capacity and the resistance to distractors were found to increase during development (Hale et al., 1997). Development of vsWM has also been related to higher activity of the WM-related areas in the frontal and parietal cortex (Klingberg et al., 2002; Kwon et al., 2002; Olesen et al., 2003). Additionally, a recent fMRI study reported lasting increase of both vsWM capacity and delay-related BOLD response following vsWM training (Olesen et al., 2004). Thus, the structural and connectivity changes integrated in the *High* and *Behavioral* network modes may also be responsible for the observed vsWM training-related changes.

Capacity limits of WM

The vsWM capacity for passive retention of information is generally considered to be of approximately four items (Luck and Vogel, 1997; Cowan, 2001), a limit which is also supported by the behavioral analyses in the present study. However, vsWM performance may also depend on rehearsal and active, attention-based maintenance processes (Awh and Jonides, 2001). The total storage capacity could therefore be constrained not only by the neuronal and synaptic properties within the cortical network but also by the additional top-down processes related to attention (Marois and Ivanoff, 2005). The exclusive maintenance of visuo-spatial information by the network model without integration of attentional mechanisms could therefore be a potential limitation of the present study.

The posterior parietal cortex has recently been proposed as the neurophysiologic correlate of vsWM storage limitation (Todd and Marois, 2004; Vogel and Machizawa, 2004). In agreement with recently reported results (Todd and Marois, 2004), the present fMRI data show that the BOLD response induced in this area was correlated with the amount of information stored in vsWM. This study adds to previous knowledge by proposing a mechanistic expla-

nation for the close relationship between BOLD response and information storage. However, it is possible that future studies could implement interventions or manipulations of the system that make the predicted BOLD response deviate from the amount of stored information.

The neuronal mechanisms underlying vsWM capacity limit

The developmental mechanisms implemented in the network have distinct contribution to the total storage capacity increase observed in the model. A higher overall connectivity, G_{EE} (A), allows a higher excitation level in the network thus increasing the total percentage of the E cells that can be simultaneously active. Increasing the contrast, J_{EE}^+ (B), increases the signal-to-noise ratio by strengthening the connectivity between neurons with similar preferred cues and lowering the connectivity strength to distant neurons. Lowering σ_{EE} (C) decreases the number of active neurons in a bump attractor allowing a higher number of bump states before the highest excitation level is reached. However, the network's dynamic stability requires a finely tuned balance between excitatory activity and inhibitory feedback, a fact that will constrain the parameter ranges. A system that reached its higher limit of excitation is marked by the spontaneous appearance of bump attractors induced by noise. Below the lower limit, the recurrent excitation will not be sufficiently strong to sustain bump activity. Thus, for a given population size, the limited excitation level will constrain the number of cues than can be simultaneously maintained by the network. Although there is no theoretical capacity limit with increased network size, the number of items maintained by the cortical circuitry underlying WM will be constrained by the available number of recruited neurons together with biophysiological factors like the maximal synaptic strength between neurons and synaptic specificity which both need to increase for higher capacity (higher J^+ and lower σ in the model). J^+ proved to be a key factor determining the multiple-item capacity of the model. Although the corresponding experimental value is yet to be determined, the value used for the behavioral mode ($J^+=13$) can be contrasted with the values ($J^+=1.62$ – 5.25) used in previous theoretical studies of one-item models (Compte et al., 2000; Tegnér et al., 2002; Wang et al., 2004). Electrophysiological measurements in monkey prefrontal cortex report a width (σ) of the neuronal tuning curves in the range of 0.12–0.15 (Constantinidis and Goldman-Rakic, 2002). Assuming a lower WM capacity for monkeys than humans, lower σ values should be expected for the human neuronal circuitry. The corresponding values for the Behavioral mode were calculated to 0.08–0.10, similar to the σ value used for the connectivity curves (0.09).

CONCLUSIONS

The structural and connectivity changes implemented in a biophysical vsWM model resulted in a significantly higher storage capacity and more robust information maintenance. Brain areas presenting similar relationship

between stored information and neural activity as predicted by the network model were identified in a group of participants performing a vsWM task. This activity was localized to the posterior parietal cortex, an area that has previously been associated with the limited information stored in vsWM (Todd and Marois, 2004; Vogel and Machizawa, 2004).

REFERENCES

- Amari S (1977) Dynamics of pattern formation in lateral-inhibition type neural fields. *Biol Cybern* 27:77–87.
- Amit DJ, Bernacchia A, Yakovlev V (2003) Multiple-object working memory: a model for behavioral performance. *Cereb Cortex* 13: 435–443.
- Amit DJ, Brunel N (1997) Model of global spontaneous activity and local structured activity during delay periods in the cerebral cortex. *Cereb Cortex* 7:237–252.
- Attwell D, Iadecola C (2002) The neural basis of functional brain imaging signals. *Trends Neurosci* 25:621–625.
- Awh E, Jonides J (2001) Overlapping mechanisms of attention and spatial working memory. *Trends Cogn Sci* 5:119–126.
- Baddeley AD, Hitch GJ (1974) Working memory. In: *Recent advances in learning and motivation* (Bower G, ed), pp 47–90. New York: Academic Press.
- Compte A, Brunel N, Goldman-Rakic PS, Wang XJ (2000) Synaptic mechanisms and network dynamics underlying spatial working memory in a cortical network model. *Cereb Cortex* 10:910–923.
- Constantinidis C, Goldman-Rakic PS (2002) Correlated discharges among putative pyramidal neurons and interneurons in the primate prefrontal cortex. *J Neurophysiol* 88:3487–3497.
- Constantinidis C, Wang XJ (2004) A neural circuit basis for spatial working memory. *Neuroscientist* 10:553–565.
- Cowan N (2001) The magical number 4 in short-term memory: a reconsideration of mental storage capacity. *Behav Brain Sci* 24: 87–114.
- Deco G, Rolls ET (2005) Attention, short-term memory, and action selection: A unifying theory. *Prog Neurobiol* 76:236–256.
- Deco G, Rolls ET, Horowitz B (2004) 'What' and 'where' in visual working memory: a computational neurodynamical perspective for integrating fMRI and single-neuron data. *J Cogn Neurosci* 16: 683–701.
- Friston KJ, Fletcher P, Josephs O, Holmes A, Rugg MD, Turner R (1998) Event-related fMRI: characterizing differential responses. *Neuroimage* 7:30–40.
- Friston KJ, Holmes AP, Poline JB, Grasby PJ, Williams SC, Frackowiak RS, Turner R (1995) Analysis of fMRI time-series revisited. *Neuroimage* 2:45–53.
- Funahashi S, Bruce CJ, Goldman-Rakic PS (1989) Mnemonic coding of visual space in the monkey's dorsolateral prefrontal cortex. *J Neurophysiol* 61:331–349.
- Fuster JM (1973) Unit activity in prefrontal cortex during delayed-response performance: neuronal correlates of transient memory. *J Neurophysiol* 36:61–78.
- Goldman-Rakic PS (1995) Cellular basis of working memory. *Neuron* 14:477–485.
- Hale S, Bronik MD, Fry AF (1997) Verbal and spatial working memory in school-age children: developmental differences in susceptibility to interference. *Dev Psychol* 33:364–371.
- Hestrin S, Sah P, Nicoll RA (1990) Mechanisms generating the time course of dual component excitatory synaptic currents recorded in hippocampal slices. *Neuron* 5:247–253.
- Hubel DH, Wiesel TN (1963) Receptive fields of cells in striate cortex of very young visually inexperienced kittens. *J Neurophysiol* 26: 994–1002.

- Huttenlocher PR (1979) Synaptic density in human frontal cortex: developmental changes and effects of aging. *Brain Res* 163:195–205.
- Jahr CE, Stevens CF (1990) Voltage dependence of NMDA-activated macroscopic conductances predicted by single-channel kinetics. *J Neurosci* 10:3178–3182.
- Jensen O, Lisman JE (1996) Novel lists of 7 ± 2 known items can be reliably stored in an oscillatory short-term memory network: interaction with long-term memory. *Learn Mem* 3:257–263.
- Kilner JM, Mattout J, Henson R, Friston KJ (2005) Hemodynamic correlates of EEG: a heuristic. *Neuroimage* 28:280–286.
- Klingberg T, Forssberg H, Westerberg H (2002) Increased brain activity in frontal and parietal cortex underlies the development of visuospatial working memory capacity during childhood. *J Cogn Neurosci* 14:1–10.
- Kwon H, Reiss AL, Menon V (2002) Neural basis of protracted developmental changes in visuo-spatial working memory. *Proc Natl Acad Sci U S A* 99:13336–13341.
- Luck SJ, Vogel EK (1997) The capacity of visual working memory for features and conjunctions. *Nature* 390:279–281.
- Luna B, Garver KE, Urban TA, Lazar NA, Sweeney JA (2004) Maturation of cognitive processes from late childhood to adulthood. *Child Dev* 75:1357–1372.
- Markram H, Lubke J, Frotscher M, Roth A, Sakmann B (1997) Physiology and anatomy of synaptic connections between thick tufted pyramidal neurones in the developing rat neocortex. *J Physiol* 500(Pt 2):409–440.
- Marois R, Ivanoff J (2005) Capacity limits of information processing in the brain. *Trends Cogn Sci* 9:296–305.
- McCormick DA, Connors BW, Lighthall JW, Prince DA (1985) Comparative electrophysiology of pyramidal and sparsely spiny stellate neurons of the neocortex. *J Neurophysiol* 54:782–806.
- Olesen PJ, Nagy Z, Westerberg H, Klingberg T (2003) Combined analysis of DTI and fMRI data reveals a joint maturation of white and grey matter in a fronto-parietal network. *Brain Res Cogn Brain Res* 18:48–57.
- Olesen PJ, Westerberg H, Klingberg T (2004) Increased prefrontal and parietal activity after training of working memory. *Nat Neurosci* 7:75–79.
- Rainer G, Miller EK (2000) Effects of visual experience on the representation of objects in the prefrontal cortex. *Neuron* 27:179–189.
- Salin PA, Prince DA (1996) Electrophysiological mapping of GABAA receptor-mediated inhibition in adult rat somatosensory cortex. *J Neurophysiol* 75:1589–1600.
- Spruston N, Jonas P, Sakmann B (1995) Dendritic glutamate receptor channels in rat hippocampal CA3 and CA1 pyramidal neurons. *J Physiol* 482(Pt 2):325–352.
- Tanaka S (2002) Dopamine controls fundamental cognitive operations of multi-target spatial working memory. *Neural Netw* 15:573–582.
- Tegnér J, Compte A, Wang XJ (2002) The dynamical stability of reverberatory neural circuits. *Biol Cybern* 87:471–481.
- Todd JJ, Marois R (2004) Capacity limit of visual short-term memory in human posterior parietal cortex. *Nature* 428:751–754.
- Vogel EK, Machizawa MG (2004) Neural activity predicts individual differences in visual working memory capacity. *Nature* 428:748–751.
- Wang XJ (1999) Synaptic basis of cortical persistent activity: the importance of NMDA receptors to working memory. *J Neurosci* 19:9587–9603.
- Wang XJ (2001) Synaptic reverberation underlying mnemonic persistent activity. *Trends Neurosci* 24:455–463.
- Wang XJ, Tegnér J, Constantinidis C, Goldman-Rakic PS (2004) Division of labor among distinct subtypes of inhibitory neurons in a cortical microcircuit of working memory. *Proc Natl Acad Sci U S A* 101:1368–1373.
- Xiang Z, Huguenard JR, Prince DA (2002) Synaptic inhibition of pyramidal cells evoked by different interneuronal subtypes in layer v of rat visual cortex. *J Neurophysiol* 88:740–750.

(Accepted 13 April 2006)
(Available online 13 June 2006)